Computers and Geotechnics 182 (2025) 107157

Contents lists available at ScienceDirect

Computers and Geotechnics

journal homepage: www.elsevier.com/locate/compgeo

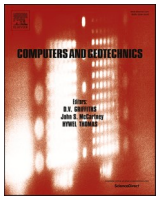

Research Paper

Predicting the uniaxial capacity of plate anchors in spatially variable clay using metamodels

Alessio Mentani [a,*], Laura Govoni [a], Christophe Gaudin [b], Phil Watson [b], Yinghui Tian [c]

[a] University of Bologna, Viale del Risorgimento 2, 40136 Bologna, Italy
[b] The University of Western Australia, 35 Stirling Highway, Crawley, Perth, Western Australia 6009, Australia
[c] The University of Melbourne, Grattan Street, Parkville, Victoria 3010, Australia

ARTICLE INFO

Keywords:
Offshore geotechnics
Plate anchors
Soil spatial variability
Ultimate capacity
Metamodelling

ABSTRACT

This paper investigates the effect of spatial variability in undrained shear strength on the uniaxial capacity of a deeply embedded plate anchor. The study was undertaken using the random field finite element method, and the results show that the ultimate uniaxial capacity is significantly influenced by strength heterogeneity, which is influenced by the different mobilised failure mechanisms and leads to a widely distributed probability of failure. Interpretation of the results also shows that it is possible to relate the statistical distribution of an operative undrained shear strength to the probability of failure of the plate, using close to constant uniaxial capacity factors. These findings simplify the assessment of plate capacity to the determination of the operative undrained shear strength, without needing to resort to computationally expensive finite element analyses. Additionally, the operative undrained shear strength obtained from random field modelling can be accurately emulated by metamodelling, which can then be used to correlate the input variables to the statistical distribution of the operative undrained shear strength. Through reference to a specific foundation geometry and set of soil variability parameters, this paper illustrates the potential of a simple and computationally cost-effective analytical procedure which, by combining random field finite element analyses and metamodels, relates site-specific field input variables to the probability of failure of a deeply embedded plate anchor in a spatially variable clay.

1. Introduction

As the offshore wind industry pushes into deeper water (nominally greater than 200 m), in part to harness better wind resources, floating solutions are considered the emerging technology for sustainable energy generation (Kumar et al., 2016). Floating turbines are moored to the seabed with anchoring systems, for which a range of solutions can be adopted (O'Loughlin et al., 2018).

Given their high efficiency, plate anchors are considered an attractive option for deep-water mooring (Randolph and Gourvenec, 2017). One installation method involves using a suction caisson to penetrate the plate to a targeted depth – upon retrieving the caisson, the anchor remains vertically inclined in the soil, and is subsequently tensioned to realise its maximum capacity or just the installation capacity if keying has not activated (Gaudin et al., 2006). Known as a Suction Embedded Plate Anchor (SEPLA), this concept can be considered for a range of offshore renewables applications, including wave energy devices (Gaudin et al., 2017) and floating wind turbines (Hallowell et al., 2018).

The undrained holding capacity of a deeply embedded plate anchor can be assessed using the capacity envelope approach, as introduced by Murff (1994). The approach was first applied to strip foundations (Ukritchon et al., 1998; Bransby and Randolph, 1998), before being extended to deeply embedded plate anchors (Merifield and Sloan, 2001; O'Neill et al., 2003). These studies analysed the foundation response when installed in fine grained soil, where the undrained shear strength, s_u, was considered either homogeneous or horizontally uniform. However, the mechanical properties of soil deposits are inherently variable, which can impact the ultimate capacity of a foundation (Griffiths and Fenton, 2001).

In general terms, the spatial variability of an engineering property can be characterised by the contribution of a deterministic trend value and a random residual. The latter represents the variability of the referred property and can be modelled by introducing an autocorrelation function that defines its spatial dependence. A random field can be

* Corresponding author.
E-mail addresses: Italyalessio.mentani2@unibo.it (A. Mentani), Italyl.govoni@unibo.it (L. Govoni), christophe.gaudin@uwa.edu.au (C. Gaudin), phillip.watson@uwa.edu.au (P. Watson), yinghui.tian@unimelb.edu.au (Y. Tian).

https://doi.org/10.1016/j.compgeo.2025.107157
Received 24 October 2024; Received in revised form 4 February 2025; Accepted 16 February 2025
Available online 26 February 2025

generated with stationarity of the statistical properties, which means that any two points in the field exhibit the same statistical behaviour, regardless of their location, i.e. the mean and variance are constants over the space. Conversely, in a non-stationary random field, the statistical properties vary spatially.

The challenge of dealing with soil variability has been investigated by many researchers. Cassidy et al. (2013) were the first to develop failure envelopes in a probabilistic framework for a strip footing resting on a clay soil, with undrained shear strength modelled as a stationary random field. The study of probabilistic failure envelopes for strip foundations on non-stationary random fields was then tackled by Shen et al. (2020), and it was subsequently demonstrated that the parameters generating a random realisation of the soil domain significantly affects uniaxial capacity, which in turn governs the size of the envelope, rather than its shape (Shen et al., 2023). With reference to plate anchors subject to uplift loading, Cai et al. (2022) demonstrated the over-conservatism that exists when using a deterministic design approach that does not account for the variability in the soil.

The aforementioned studies have quantified the probability of failure of shallow foundations for selected combinations of input parameters required to generate a random field of soil strength. The outcomes of these studies are typically given in form of tables or charts, providing guidelines for site-specific design, where it is likely that the input parameters are different from the examined selected combinations. In contrast, this study aims to provide a generalisation of the approach such that the probability of failure of the foundation can be predicted for any combination of the input variables, by employing suitably devised equations.

More specifically, this study addresses the probability of failure of a deeply embedded plate anchor in a non-stationary random field of s_u under uniaxial vertical, V and horizontal load, H, and overturning moment, M (Fig. 1). The determination of uniaxial capacity is essential in defining the interaction diagrams that describe the ultimate response of a plate anchor under combined loading conditions, whose dimensionless representation requires uniaxial ultimate capacity to be known either in a deterministic (Vulpe et al., 2014) or probabilistic (Cassidy et al., 2013; Shen et al., 2023) framework.

The uniaxial capacities were investigated using the Random Field Element Method (RFEM, Fenton and Griffiths, 2008) with non-stationary fields of undrained shear strength mapped onto the finite element mesh. The methodology adopted for generating random realisations was analysed to identify an operative s_u that might represent the soil spatial variability, while also accounting for the load path assigned to the plate.

The problem of plate anchor capacity was then analysed through a probabilistic framework, adopting the Polynomial Chaos Expansion (PCE) metamodelling technique. Metamodels are numerical techniques used to emulate the response of an original (more complex) model at negligible computational cost. Through metamodels, the stochastic processes within the original model are emulated by an approximation function representing the relationship between input variables and output responses. Different metamodelling techniques have been successfully employed in geotechnical engineering over the last few years, such as polynomial chaos (Shen et al., 2020; Mentani et al., 2023), Gaussian process (Suryasentana et al., 2024a), random forest (Zhang et al., 2020) and artificial neural networks (Suryasentana et al., 2024b). Interest in the use of these methods is increasing as they provide a fast and efficient means to perform uncertainty quantification.

With reference to a deeply embedded plate anchor in a spatially variable clay soil, the specific aims of this study are as follows:

1. To investigate the effect of the soil spatial variability on ultimate uniaxial capacity, and identify the uniaxial capacity factors;
2. To develop a generalised approach to assess the statistical distribution in ultimate uniaxial capacity;
3. To optimise the metamodeling procedure in order to reduce computational cost and implementation complexity.

2. Methodology

2.1. Details of anchor geometry

The uniaxial ultimate capacity (either vertical, V_u, horizontal, H_u, and moment M_u) of a deeply embedded plate anchor in undrained loading conditions was evaluated by employing the random finite element method RFEM in combination with the use of metamodelling. Two-dimensional plane strain conditions were prescribed to a plate anchor of width $B = 1$ m and thickness $t = B/20$, which was horizontally

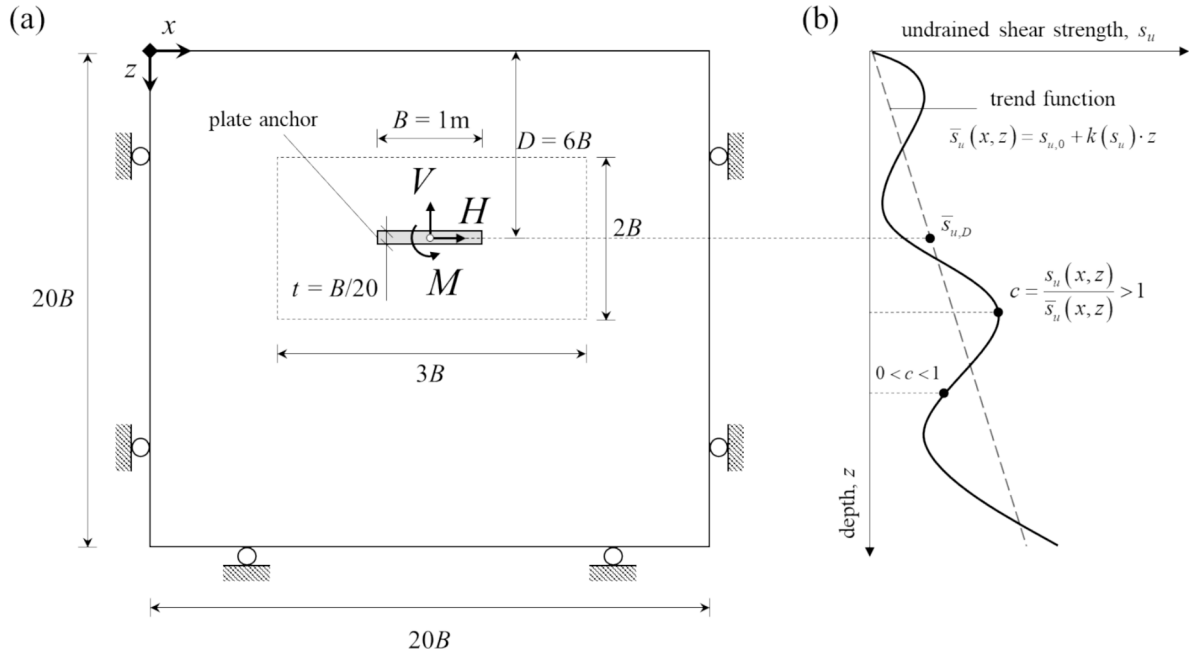

Fig. 1. Model geometry and idealised plot of the undrained shear strength, s_u, with depth.

wished in place in a 20*B* wide and 20*B* deep domain (Fig. 1a). The plate was embedded at 6*B* to ensure deep failure mechanisms formed in response to the applied loads (Yu et al., 2010). Within the domain the undrained shear strength, s_u, was spatially varied using non-stationary random fields (Fig. 1b).

2.2. Random field modelling

A non-stationary random field can be defined as the product of a stationary random field and a mean trend function (Lumb, 1966). Thus, in the two-dimensional space (x, z) of Fig. 1, a random realisation of s_u can be built as:

$$s_u(x,z) = \bar{s}_u(x,z)\cdot\Delta_c(x,z) \tag{1}$$

where Δ_c is a stationary random field; and $\bar{s}_u$ is a depth-wise trend function assumed as:

$$\bar{s}_u(x,z) = s_{u,0} + k(s_u)\cdot z \tag{2}$$

where $s_{u,0}$ is the undrained strength at the mudline; and $k(s_u)$ is the strength gradient (Fig. 1b).

In this project a stationary random field was built for the non-dimensional undrained shear strength $c = s_u/\bar{s}_u$ using a log-normal distribution; which was done to avoid the generation of negative soil strengths. The field was first generated as a Gaussian random field, $G(x, z)$, with standard normal distribution (i.e. zero mean and unit variance) and then transformed to the log-normal distributed field using the following expression:

$$\Delta_c(x,z) = \exp[\mu_{\ln c} + \sigma_{\ln c} G(x,z)] \tag{3}$$

where $\mu_{\ln\ c}$ and $\sigma_{\ln\ c}$, are the statistical properties of the log-normal distributed field. Those can be related to their linear statistical properties, μ_c and σ_c, as:

$$\mu_c = \exp\left(\mu_{\ln c} + 0.5\sigma^2_{\ln c}\right) \tag{4}$$

$$\sigma_c = \exp\left(2\mu_{\ln c} + \sigma^2_{\ln c}\right)\left[\exp\left(\sigma^2_{\ln c}\right) - 1\right] \tag{5}$$

$$\mathrm{COV}(c) = \frac{\sigma_c}{\mu_c} \tag{6}$$

where COV(c) is the coefficient of variation. It can be demonstrated that COV(c) = COV(s_u), and as such a set of values of the statistical properties that satisfy Eq. (4) to Eq. (6) can be evaluated for a targeted value of COV (s_u) with a least squares minimization approach. This allows generation of the log-normal distributed field (Δ_c) through Eq. (3). In this study, COV(s_u) was assumed constant in the space, which is a common practice in offshore geotechnical applications (Wu et al., 2020, Yi et al., 2020, Cai et al., 2022, Chen et al., 2023, Shen et al., 2023).

The stationary Gaussian field, $G(x,z)$, was generated with a spectral representation method, following the approach detailed in Räss et al. (2019), whereby a squared exponential autocorrelation function was adopted to define the correlation structure of the field:

$$\rho(x,z) = \exp\left[-\left(\frac{x_i - x_j}{\delta_x}\right)^2 - \left(\frac{z_i - z_j}{\delta_z}\right)^2\right] \tag{7}$$

where (x_i, z_i) and (x_j, z_j) are two grid points in the 2D space; δ_x and δ_z are the correlation lengths in the horizontal and vertical directions, respectively. The latter are commonly expressed in terms of the horizontal and vertical scale of fluctuation of s_u (i.e. $\theta_x(s_u)$ and $\theta_z(s_u)$), and for a squared exponential autocorrelation function their relationship is $\theta = \pi^{0.5}\,\delta$ (Phoon & Kulhawy, 1999).

According to the above procedure, the realisation of a non-stationary random field of s_u therefore requires the definition of five input variables: the undrained shear strength at the mudline, $s_{u,0}$; the gradient of the trend function, $k(s_u)$; the coefficient of variation, COV(s_u); and the horizontal and vertical scale of fluctuation, $\theta_x(s_u)$ and $\theta_z(s_u)$.

2.3. Finite element modelling

The finite element (FE) analyses were carried out with the commercial finite element package ABAQUS (Dassault Systémes, 2020). With reference to Fig. 1a, horizontal and vertical displacements were restrained at the lateral and bottom edges of the mesh. The soil was modelled using 4-node bilinear plane strain elements, with a structured mesh of minimum size set equal to $t/4$ in proximity of the plate. A transition mesh was used in an area of 3*B* x 2*B* centred on the plate, with a coarser non-structured mesh used outside this area – an approach that reduced the total element number to about 24,000.

A linear-elastic perfectly-plastic material (Young modulus $E = 500s_u$ and a Poisson ratio of 0.49) with a Tresca failure criterion was prescribed to each soil element. The undrained shear strength, s_u, was assigned according to the generated random fields. The anchor was modelled as a rigid element with its reference point located at its centroid, with a fully bonded contact assumed at the interface between the plate and the soil (a common approach when simulating undrained conditions, per Merifield et al., 2001). The uniaxial V, H and M were investigated by assigning (respectively) vertical, horizontal and rotational velocity boundary conditions at the reference point, with the ultimate capacity (V_u, H_u, M_u) taken as the value at which the load–displacement curve reached a clear plateau.

2.3.1. Interpretation of the results

The numerical analyses were interpreted in terms of capacity factors as follows:

$$N_{cV} = \frac{V_u}{BLs_u^{(V)}}$$
$$N_{cH} = \frac{H_u}{BLs_u^{(H)}} \tag{8}$$
$$N_{cM} = \frac{M_u}{B^2Ls_u^{(M)}}$$

where L is the anchor length (taken as unity in plane strain conditions), and $s_u^{(V)}$, $s_u^{(H)}$ and $s_u^{(M)}$ are the average s_u computed in the non-stationary realisation of s_u by considering the soil elements along the kinematic failure mechanisms for the anchor in homogeneous clay, as proposed by O'Neill et al. (2003) and illustrated in Fig. 2 within a 3*B* x 2*B* area.

This normalisation differs from previous studies, which adopt the value of undrained shear strength calculated by the trend function at the anchor reference point $\bar{s}_{u,D}$ (Wu et al., 2020; Cai et al., 2022; Chen et al., 2023).

Failure mechanisms in homogeneous clay may differ from those that are mobilised in a soil characterised by a spatially variable strength, leading to different capacity values (Li et al., 2015; Yi et al., 2020; Wu et al., 2020, Cai et al., 2022). Example displacement fields, referring to three different random realisations (that are consistent with this study), are depicted in Fig. 3 for the anchor subjected to controlled displacements until failure for vertical (Fig. 3a), horizontal (Fig. 3b), and moment (Fig. 3c) conditions of loading.

As observed, while the overall shape is broadly maintained for the same load path, there are changes in extent – which are most obvious for vertical load. The potential loss in symmetry is also clearly shown, as the mechanisms search for weaker load paths.

Accordingly, $s_u^{(V)}$, $s_u^{(H)}$ and $s_u^{(M)}$ calculated using the mechanisms in Fig. 2 may be regarded as an approximation of the values associated with more general failure mechanisms, as demonstrated in Fig. 3. However, they have the advantage of being easily calculated, as the mechanisms are known a priori and the results of more time consuming

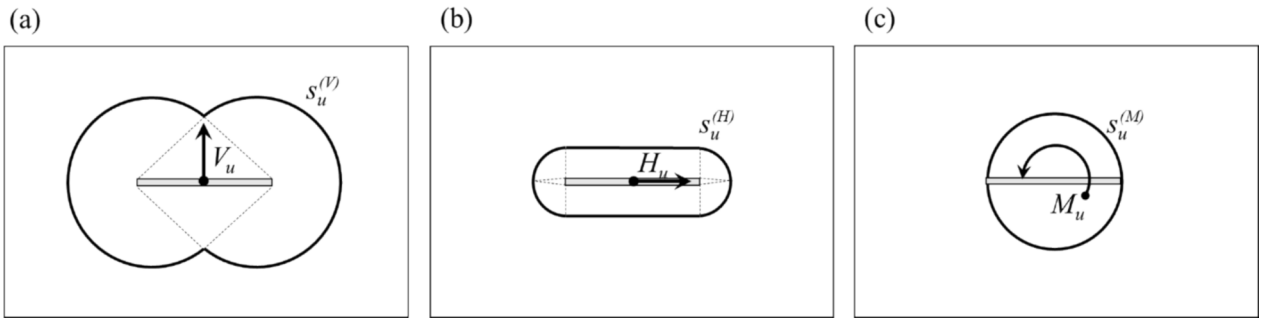

Fig. 2. Kinematic failure mechanisms (redrawn after O'Neill et al., 2003) of a plate anchor subjected to controlled displacements for the calculation of: (a) horizontal load; (b) vertical load; and (c) moment.

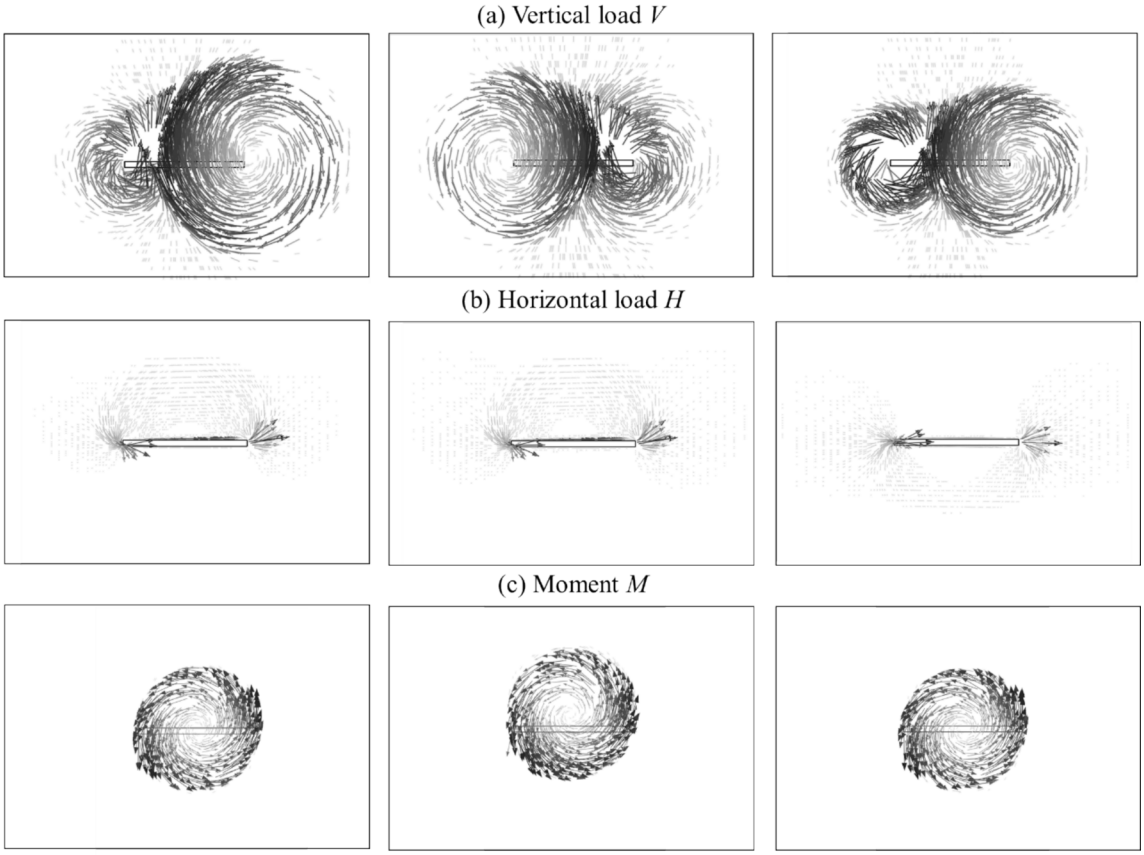

Fig. 3. Displacement fields (at failure) of the plate anchor subjected to controlled displacements, as observed for three different random realisations: (a) vertical load; (b) horizontal load; and (c) moment.

RFE analyses are not required. This assumption allowed the development of a simple to implement and computationally cost-effective procedure for the computation of uniaxial capacity values. As it will be shown in Section 5, the use of these values in the procedure ensures a very good fit to the RFE results. The undrained shear strengths (calculated using Fig. 2) are hereinafter referred to as operative strengths.

2.4. Polynomial Chaos Expansion (PCE) metamodelling

A metamodel is a mathematical function that approximates the response of a more computationally expensive numerical model. The approximation function describes the link between the inputs and identified outputs of interest in the original numerical model.

The procedure (as adopted here) for generating a metamodel is described in more detail in Mentani et al. (2023). In general terms, a numerical problem consists of a number n of input variables and m output variables, which can be collected by the vectors $\boldsymbol{x}^{(i)}=\{x_j \mid j=1, 2, \ldots, n\}$ and $\boldsymbol{y}^{(i)}=\{y_j \mid j=1, 2, \ldots, m\}$, respectively. The metamodel is then built from a dataset of input combinations and their corresponding model outputs, whereby the input variables are sampled to generate a training dataset of size N, $\boldsymbol{X}=\{\boldsymbol{x}^{(i)} \mid i=1, 2, \ldots, N\}$, while the numerical outputs are stored in the model response vector $\boldsymbol{Y}=\{\boldsymbol{y}^{(i)} \mid i=1, 2, \ldots, N\}$. The metamodel is then a function that returns a vector $\boldsymbol{Y}^*$ that approximates the model response vector.

In the case of PCE metamodeling, the function is built using a set of orthogonal polynomials in a spectral expansion of the input variables (Soize and Ghanem, 2004) generating a Fourier-like series as:

$$\boldsymbol{Y}^* = g(\boldsymbol{X}) = \sum_{k=1}^{K} \alpha_k \psi_k(\boldsymbol{X}) \approx \boldsymbol{Y} \tag{9}$$

where K is the size of the PCE; $\Psi_k(\boldsymbol{X})$ are multivariate orthonormal polynomials in the input vector; and α_k are coefficients.

In the present study, PCE was used to predict the statistical distribution of the operative strengths that correspond to specific combinations of random field input parameters.

Implementing a PCE equation requires:

1) Identification of the type of polynomial basis, $\Psi_k(\boldsymbol{X})$;
2) Definition of a truncation scheme to set the size K;
3) Computation of equation coefficients, α_k.

2.4.1. Setup of the PCE mathematical model

Choosing the family of polynomials to be used in PCE can be linked to the probability density function (PDF) of the input variables, which in turn reflects the available training dataset – with the type of orthonormal polynomial basis associated to standard distribution types, as detailed by Sudret (2008).

While the PCE equation would exactly represents the original model function if an infinite series was considered (i.e. $K = \infty$), this is impractical and the series must be truncated to a finite number. In this study, the number of series was taken with consideration of the number of input variables, n, and of the maximum degree of the polynomials, p. In a standard truncation scheme, the total degree of the multivariate polynomial is set smaller than or equal to a given p, per Le Gratiet et al. (2015), which leads to a size K of the PCE equation as follows:

$$K = \frac{(n+p)!}{n!p!} \tag{10}$$

This implies that the number of coefficients to be computed in Eq. (9) will drastically increase if a large number of input variables is involved, or if higher degrees of polynomial are targeted.

The coefficients of the PCE can be estimated using intrusive or non-intrusive methods. In this study, a non-intrusive approach was employed, which involved a least-squares minimization technique to compute the coefficients as follows:

$$\alpha = \operatorname{argmin} \frac{1}{N} \sum_{i=1}^{N} \left[\boldsymbol{y}^{(i)} - \sum_{k=1}^{K} \alpha_k \psi_k \left(\boldsymbol{x}^{(i)} \right) \right]^2 \tag{11}$$

In order to solve Eq. (11), the number N of model evaluations in the training dataset is required to be larger than the number of unknown coefficients, K. For a problem to be well-posed, Le Gratiet et al. (2015) suggested a rule of thumb of $N \approx 2$–$3\ K$.

However, when used with a standard truncation scheme, this can pose problems if the original numerical model is computationally expensive and a large amount of data is required. To overcome this difficulty, a so-called 'sparse' scheme can be employed (Blatman and Sudret, 2010), in which only the significant coefficients in the PCE approximation function are identified by considering a cut-off value, $\varepsilon_{\text{cut-off}}$. This allows to reduce the number of terms in the full PCE representation. Blatman and Sudret (2010) proposed the least angle regression (LAR) approach for building a sparse PCE, which comprises an iterative procedure whereby the coefficients are initially computed using a standard setup. If a coefficient is lower than the cut-off value, the relevant polynomial is discarded by the PCE equation and the coefficients are re-computed – and the operation continues until $q = \min(K, N–1)$ coefficients have been computed.

2.4.2. Accuracy of the PCE

The accuracy of the PCE was assessed using the Leave-One-Out (LOO) cross-validation technique, which involves partitioning an initial sample of size N into a training sample of size (N–1) and a validation sample consisting of the discarded input/output pair. The coefficients are computed using the training set and the PCE developed without the i^{th} pair (i.e. $g^{PCE\backslash i}$) is employed to predict the output for the validation sample. The procedure is iterated for all N combinations, and the PCE accuracy can be quantified via a normalised factor defined as:

$$Q^2_{LOO} = 1 - \varepsilon_{LOO} = 1 - \frac{\frac{1}{N}\sum_{i=1}^{N} \left[\boldsymbol{y}^{(i)} - g^{PCE\backslash i}\left(\boldsymbol{x}^{(i)} \right) \right]^2}{\mathrm{Var}(\boldsymbol{Y})} \tag{12}$$

where $\mathrm{Var}(\boldsymbol{Y})$ is the variance of the model response vector. This accuracy score ranges from 0 to 1, where values closer to 1 represent better PCE performance.

3. Random field operative undrained shear strength

3.1. Random field generations

Non-stationary spatially variable fields of s_u were generated using three input ($k(s_u)$, $\mathrm{COV}(s_u)$, $\theta_z(s_u)$) from the five variables introduced in Section 2.1. For undrained shear strength at mudline, $s_{u,0}$, a constant value of 0.1 kPa was assigned, whereas the horizontal scale of fluctuation, θ_x, was scaled from the vertical, θ_z ($\theta_x = 10\ \theta_z$). These conditions were selected as they are believed to be representative of a range of deepwater offshore sites (Yi et al., 2020, Ching & Schweckendiek 2021). The selected input variables were assigned a realistic range according to the most relevant literature references (and are summarised in Table 1) – $k(s_u)$ was taken as being between 1 and 2 kPa/m, as recommended by Cai et al., 2022; a range between 0 and 0.5 was adopted for the coefficient of variation, as used in similar studies (Cassidy et al., 2013; Cai et al., 2022; Shen et al., 2023); and the variation in θ_z was set according to observations in Cami et al. (2020) and Ching & Schweckendiek (2021).

For each random combination of the input variables, infinite fields of s_u can be generated. As an example, Fig. 4 shows the output of two realisations, referred to as Field 1 and Field 2, which were created with the same combination of inputs ($k(s_u) = 1.89$ kPa, $\mathrm{COV}(s_u) = 0.39$, $\theta_z(s_u) = 4.43$ m). Here, Fig. 4a shows the distribution of s_u over the entire soil domain for Field 1, while Fig. 4c focuses on the distribution closer to the anchor position. Fig. 4b and 4d show the same outputs for Field 2. Looking at the area around the anchor, the range of variation in s_u is 10 kPa/m to 20 kPa/m for Field 1, and 7 kPa/m to 14 kPa/m for Field 2. The s_u at the anchor reference point is different within the two fields, and not the same as the value determined by the trend function ($\bar{s}_{u,D} = 11.46$ kPa, Fig. 4c and 4d). Fig. 4c and 4d also show the failure mechanism associated with full-flow rotational failure of the plate for a homogeneous soil (Fig. 2c). The calculation of $s_u^{(M)}$, determined as the mean of the s_u values in each soil element crossed by the failure planes, is thought to provide a more realistic representation of the soil strength at the anchor location yielding values of 16.28 KPa and 9.72 KPa for Field 1 and Field 2, respectively. Similar values were measured for $s_u^{(V)}$ (determined with the mechanism of Fig. 2a and providing $s_{u,}1^{(V)} = 16.25$ kPa and $s_{u,}2^{(V)} = 10.07$ kPa) and $s_u^{(H)}$ (determined with the mechanism of Fig. 2b and providing $s_{u,}1^{(H)} = 17.11$ kPa and $s_{u,}2^{(H)} = 10.04$ kPa). The difference of these values with respect to $\bar{s}_{u,D}$ suggests the operative strengths can be more representative of the relevant random field. It is also apparent that for any field realised using a single set of input variables, a different set of operative strengths will be computed, which supports statistical analysis –as described in the following section.

Table 1
Input variables and range of variation.

Input	Unit	Range
$k(s_u)$	kPa/m	1.0–2.0
$\mathrm{COV}(s_u)$	–	0.0–0.5
$\theta_z(s_u)$	m	0.0–10.0

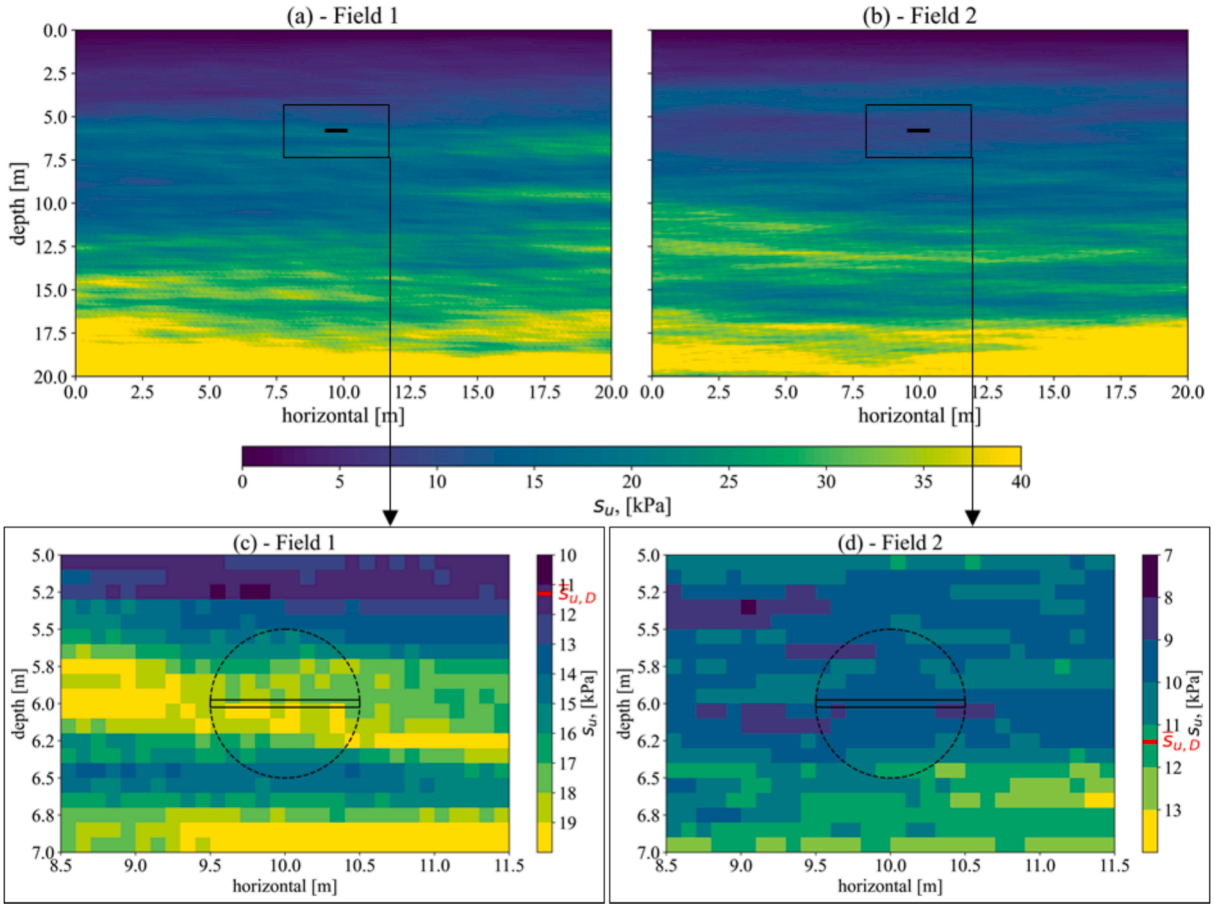

Fig. 4. Spatially variable domains of s_u obtained with: $k(s_u) = 1.89$ kPa, $\mathrm{COV}(s_u) = 0.39$, $\theta_z(s_u) = 4.43$ m with overturning moment failure mechanism of Fig. 2c.

3.2. Random fields and operative undrained shear strength

The heterogeneity of s_u for a single combination of input variables was first explored. In this case, 300 realisations were generated using $k(s_u) = 1.51$ kPa, $\mathrm{COV}(s_u) = 0.28$, $\theta_z(s_u) = 7.99$ m. For each realisation the values of the operative strengths ($s_u^{(V)}$, $s_u^{(H)}$, $s_u^{(M)}$) and their average $s_u^{(a)}$, were first computed before being divided by $\bar{s}_{u,D}$ to yield the dimensionless strengths $s_u^{(V)*}$, $s_u^{(H)*}$, $s^{(M)*}$ and $s_u^{(a)*}$ (e.g. $s_u^{(V)*} = s_u^{(V)}/\bar{s}_{u,D}$). Probability density functions (PDF) fort each term are shown in Fig. 5.

In Fig. 5, the four PDFs have been interpolated by a log-normal distribution curve:

$$p(x, f_s) = \frac{1}{x f_s \sqrt{2\pi}} \exp\left[-\frac{1}{2} \left(\frac{\ln x - \ln f_m}{f_s} \right)^2 \right] \tag{13}$$

where f_m and f_s are the scale and shape parameters of the distribution, which represent the mean and the standard deviation of the natural logarithm of the x variable.

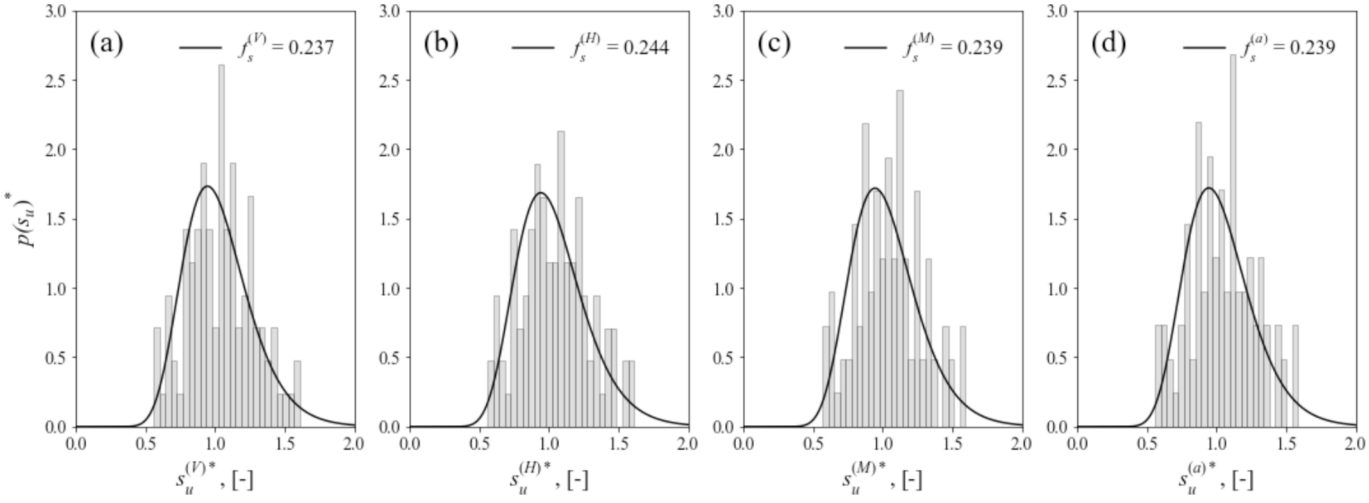

Fig. 5. PDF of the normalised operative strengths measured for: (a) vertical, (b) horizontal, and (c) moment failure mechanisms; and (d) average of the three values.

The scale parameter was set to one, as it was shown to have negligible variation, while the shape parameters that fit the distributions were calculated as $f_s^{(V)} = 0.237$, $f_s^{(H)} = 0.244$, $f_s^{(M)} = 0.239$, showing a good agreement with the average shape parameter $f_s^{(a)} = 0.239$. Consequently, the shape parameter, $f_s^{(a)}$, was used as a statistical property describing the probability of occurrence of the operative s_u, which is in turn used for the evaluation of the uniaxial capacity factors (Eq. (8)).

3.3. Sensitivity analyses

A sensitivity study was carried out using three random combinations of the selected inputs, with $N_R = 500$ realisations generated for each case. The investigation also considered the influence on the measured value of the grid size, d_m, of the random domain – being the minimum distance between two grid points in the space (i.e. i and j in Eq. (7), d_m was varied from a minimum of 0.1 m ($d_m = B/10$) to a maximum of 1 m ($d_m = B$). The $f_s^{(a)}$ parameter was then calculated by considering different sizes of N_R, from a minimum of 10 to the maximum of 500, as illustrated in Fig. 6.

The results show large variations in the computed values when small sample sizes are considered ($N_R < 100$), with marked differences also occurring when the random realisations have been generated with different grid sizes. In comparison to the mean value of $f_s^{(a)}$ determined for all four grid sizes and $N_R = 500$, the deviations fall within a 5 % limit once $N_R \geq 300$. This is broadly consistent with observations made by Li et al. (2015) and Cai et al. (2022), who identified 400 realisations as being needed to obtain stable statistical properties of anchor holding capacity.

In this study, $N_R = 300$ random realisations were considered for computing the shape parameter of $s_u^{(a)}$, with a resolution grid $d_m = 0.5$ m. This selection also came from consideration of the computational cost required for generating the random realisations, as the 50 h required to build 300 domains with $d_m = 0.1$ m reduced to less than 2 h for $d_m = 0.5$ m. It is worth noticing that the procedure could be easily extended to a more refined grid resolution and larger sample sizes.

4. Uniaxial capacity factors

4.1. Random FE modelling of the plate uniaxial capacities

A total of 15 randomly selected input combinations were considered to assess plate uniaxial capacity, sampled from range in input variable reported in Table 1. For each combination, 20 random soil realisations were generated. The domains were implemented in the FE model and a total of 300 RFEA were run for each of the three uniaxial loading conditions.

Fig. 7 presents histograms and cumulative density functions (CDF) for the ultimate uniaxial capacities obtained with the RFEA. The data were first plotted in terms of probability of occurrence of the measured loads (Fig. 7a, 7b and 7c), which showed high variability of the RFEA outcomes – which is a consequence of the different input combinations considered in the selection, as well as of the randomness of the generated domains.

The same numerical results were then plotted as capacity factors, calculated using the undrained shear strength at the anchor reference point (Fig. 7d, 7e, 7f). In this case, the distribution shapes closely resemble the dimensional outcomes, as the value of $\bar{s}_{u,D}$ fails to capture the spatial variation of shear strength in the random domains (as anticipated in Section 3.1). It also worth noting that the distribution of vertical capacity factor was similar to the findings obtained by Cai et al. (2022), who implemented an approach similar to this study.

Finally, the results of the RFEA were interpreted using the operative undrained shear strength, $s_u^{(a)}$, to compute the capacity factors (Fig. 7g, 7h, 7i) according to Eq. (8). This normalisation reduces the variability in capacity factors, leading to values as follows:

$$\begin{aligned} N_{cV} &= 11.8 \\ N_{cH} &= 3.22 \\ N_{cM} &= 1.65 \end{aligned} \tag{14}$$

These are close to values observed for plates in homogeneous clay (Elkhatib and Randolph, 2005), and also aligns with findings obtained by Stanier and White (2019, which showed that the capacity factors collapse to approximately constant values using the mobilised shear strength. However, the computation of the mobilised shear strength requires the results of RFEA.

The choice to use a priori kinematic failure mechanisms was governed by the need to adopt a procedure that allowed calculation of the probability of failure of the anchor, without having to run the computationally intense RFEA. Use of the operative $s_u^{(a)}$ allowed the identification of constant capacity factors, which was not possible when using $\bar{s}_{u,D}$. The constant capacity factors then allow for a quick yet accurate estimate of the uniaxial capacity of the plate.

4.2. PCE metamodelling of the operative shear strength

As described in Section 3, and with reference to a single combination of the three selected inputs, the operative $s_u^{(a)}$ could be predicted using a log-normal distribution defined by a single statistical measure, i.e. the shape parameter, $f_s^{(a)}$. In order to predict the operative $s_u^{(a)}$ for any random combination of inputs, the PCE metamodelling technique was employed.

In this case, the problem selected for the PCE study consisted of $n = 3$ input variables ($k(s_u)$, $\mathrm{COV}(s_u)$, $\theta_z(s_u)$) and $m = 1$ target output ($f_s^{(a)}$). A training dataset of size $N = 200$ was generated by sampling the three inputs within their ranges. The Latin Hypercube Sampling (LHS) technique was then used, with each variable set to have a uniform distribution. The method divides all variables in N equal probability intervals, with each interval filled with one input combination – with an illustration provided in Fig. 8. Consistent with the sensitivity analysis in

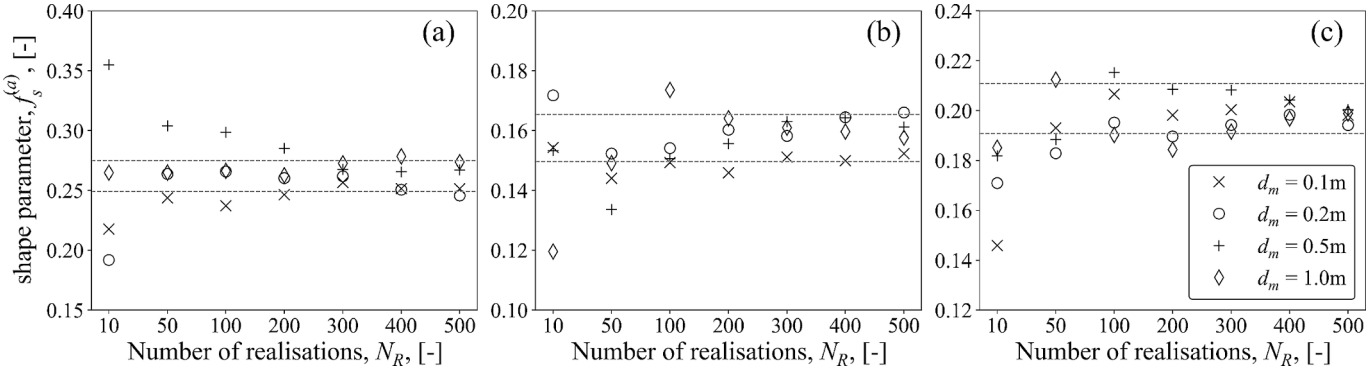

Fig. 6. Shape parameters of the operative s_u calculated as a function of the considered number of realisations, N_R, and of the grid size, d_m.

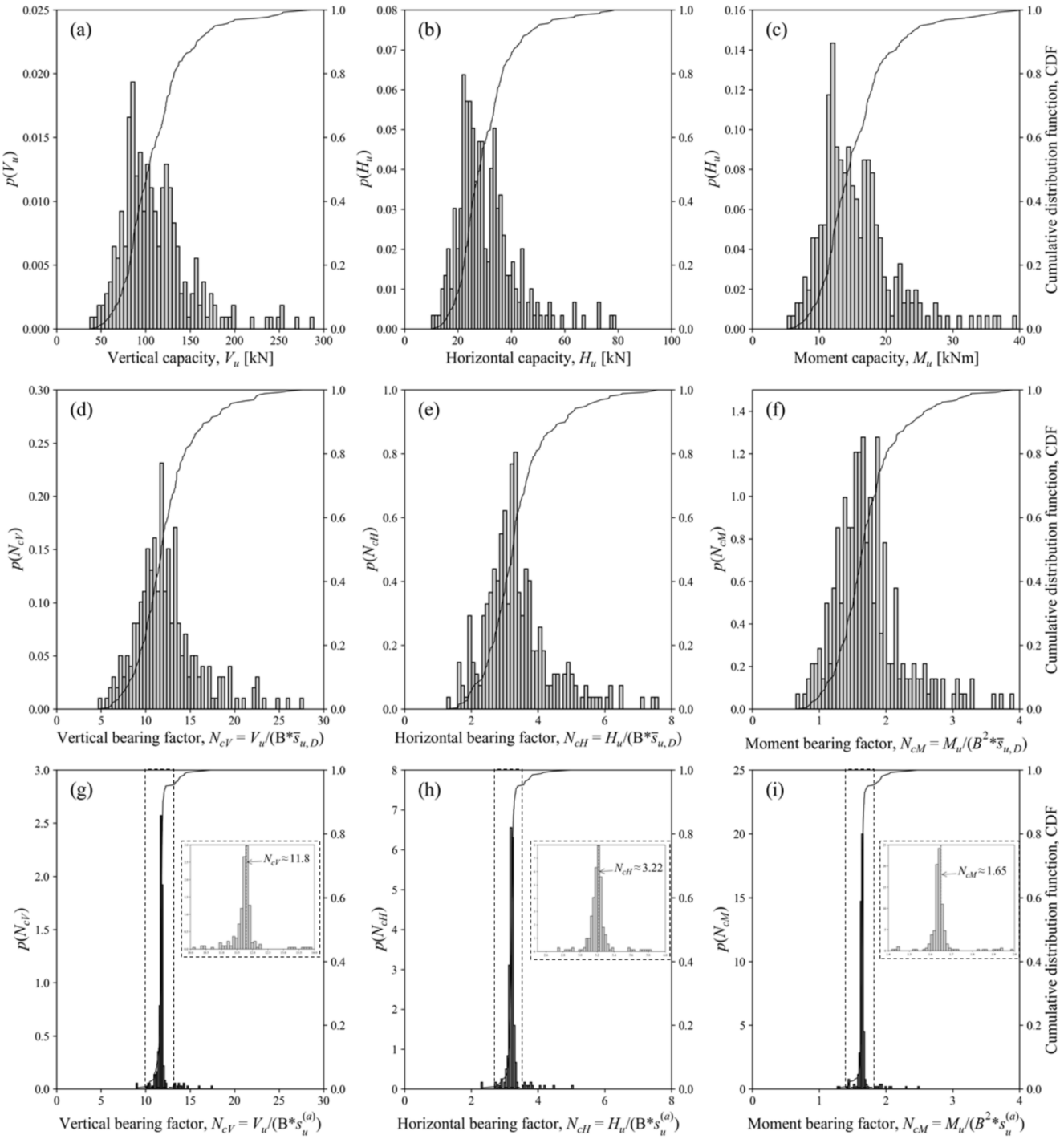

Fig. 7. Histograms and empirical CDF of the uniaxial capacities of the plate anchor in spatially variable clay: (a), (b), and (c), magnitude of the measured loads; (d), (e), and (f), capacity factors normalised by $\bar{s}_{u,D}$; (g), (h), and (i), capacity factors normalised by $s_u^{(a)}$.

Section 3, $N_R = 300$ random fields were generated for each input pair, and the relevant $f_s^{(a)}$ parameters were computed and stored in the model response vector, $\boldsymbol{Y}$.

4.2.1. PCE development and accuracy

Development of the PCE requires the definition of three model options. In this study, the Legendre polynomials were adopted as the input were sampled with uniform distributions in the LHS method. The standard truncation scheme was employed to build the equation, and the coefficients were computed according to Eq. (11). Working with this configuration, hereby named 'standard PCE', it was possible to build a PCE with a maximum degree $p = 6$ of the polynomials considering $N \approx 2$–$3\ K$. A 'sparse PCE' was also developed by implementing the LAR technique in the computation of the coefficients, which forced the multivariate polynomials to reach higher degrees. The PCE equations were built with both approaches and the LOO method was used for measuring their accuracy.

Fig. 9a presents the measured accuracies of the two PCEs as function of the maximum degree of the polynomials. The standard PCE reached a peak accuracy of $Q^2 = 0.963$ for $p = 3$, with the performance deteriorating when polynomial of higher degree were used. The sparse PCE gave slightly improved accuracy ($Q^2 = 0.966$) when polynomials up to

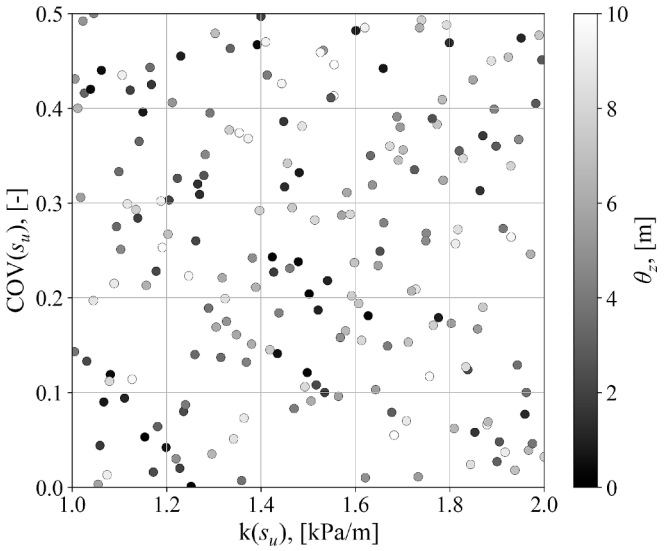

Fig. 8. LHS sample of size $N = 200$ of the three input variables.

degree $p = 6$ were implemented. Details on the significant polynomials considered after applying the LAR approach were reported in Appendix A, together with the computed coefficients. In Fig. 9b the predictions of the sparse PCE that maximised the accuracy are compared to the shape parameters computed by the generated random fields. The plot clearly highlights the quality of the PCE predictions, which generally fall close, to the best-fit represented by the continuous line. The accuracy of the sparse PCE was also highlighted in Fig. 9c, which reported the distribution of the residuals of the $N = 200$ predictions – and shows that the mean of the residuals is approximately zero (i.e. $\mu = 2*10^{-5}$) with negligible standard deviation (i.e. $\sigma = 0.022$). While not presented, similar outcomes were obtained for the standard PCE.

Given their accuracy, it can be concluded that PCEs can provide a quick and reliable estimate of the probability of the operative $s_u^{(a)}$. These can be obtained without the need to generate random realisations for any combination of the selected inputs, and in turn, can be linked to the probability of the respective uniaxial capacities of the plate anchor through constant capacity factors.

5. Application of the approach

The overall aim of this study was to identify an approach for predicting the probabilistic uniaxial capacities of a plate anchor in spatially variable soils. The approach is based on an operative undrained shear strength, which represents a specific non-stationary random field. Fig. 10 summarises the methods (described further below) used in achieving the objective of the study. All methods begin by estimating the three input variables. It is worth noting that the identification of these variables can be easily achieved through standard site investigation techniques.

Method 1 represents the standard RFE approach, for which multiple random fields (e.g. $N_R = 300$ in this study) have to be generated for the relevant inputs that characterise the site. Each soil realisation needs to be mapped onto an FE model, and simulations run to compute the ultimate capacities, whose distributions can be interpreted with a log-normal distribution (as in this study). This process is computationally expensive, as it requires time to generate the random fields (i.e. t_{RF}) and conduct the RFEA (t_{RFEA}). Assuming $N_R = 300$ (see Section 3.3), the $t_{RF} \approx 2$ h and $t_{RFEA} \approx 24$ h for each load path. Additionally, the implementation and data interpretation of Method 1 is rather complex and itself time consuming.

As an alternative, Method 2 involves computing the operative undrained shear strength, $s_u^{(a)}$, once the soil realisations are generated (i.e. after Step 2 of Method 1). Observed $s_u^{(a)}$ can be fitted to a log-normal distribution (Eq. (13) to determine the best-fit scale parameter $f_s^{(a)}$. The distribution of $s_u^{(a)}$ can then be scaled to the respective uniaxial capacity of the plate via the scale parameter f_m (Eq. (13)) by using the constant capacity factors determined in the previous section (Eq. (14)). This method allows estimates for the probability of each uniaxial capacity to be derived with reduced computational cost, as the FE stage analysis can be bypassed though maintaining the laborious random field modelling.

Based on the findings of this study, the computational time cost can be further (significantly) reduced by using a metamodel approach. Defined as Method 3, the inputs for the site can be directly used to compute $f_s^{(a)}$ with the PCE equation (Appendix A). As in Method 2, this can then be used to plot distributions of the plate uniaxial capacities. This further optimises the process by eliminating both the need to generate the random fields as well as to perform the FEA study, thereby drastically reducing the computational cost and the implementation complexity.

5.1. Proof of concept of the proposed approaches

The three methods were tested for a combination of the input variables: whereby the gradient of the trend function was set to 1.2 kPa/m, with a coefficient of variation of 0.3 and a vertical scale of fluctuation of 2.5 m. The vertical uniaxial capacity was then analysed, with a deterministic capacity computed from Eq. (8) as $V_{u,det} = 86.14$kN.

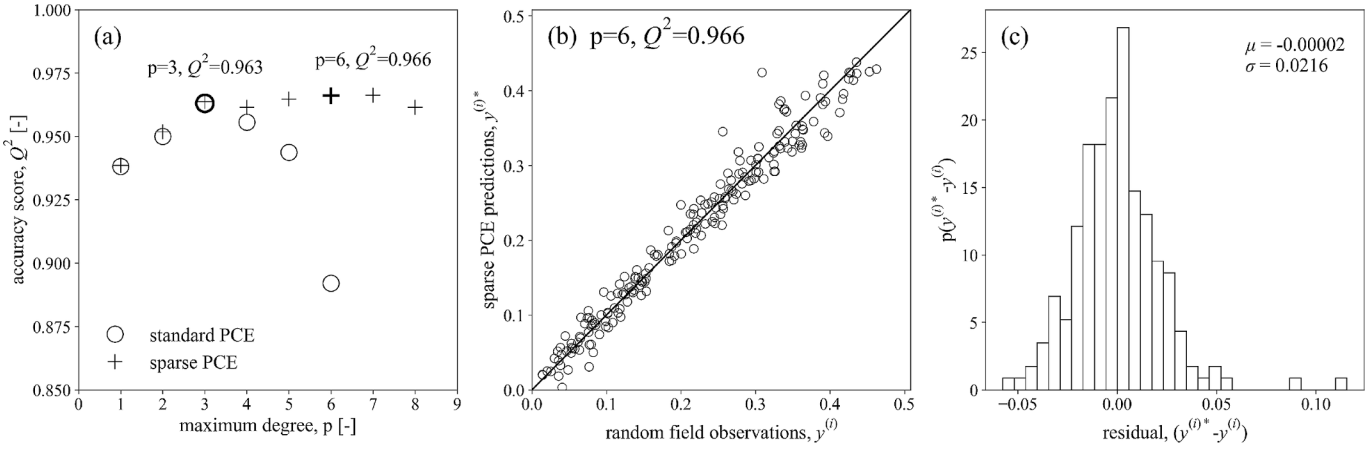

Fig. 9. Accuracy of the developed PCEs: (a) accuracy score as function of the maximum degree of the polynomials for the standard and sparse PCE; (b) comparison of the sparse PCE predictions Vs observed values from the generated random fields; (c) PDF of the residuals of the sparse PCE.

Method 1 – RFE approach	Method 2 – approach with RF generation	Method 3 – metamodel approach
1. compute the input variables from the site information: $\{k(s_u), \mathrm{COV}(s_u), \theta_z(s_u)\}$ 2. generate N_R random fields → t_{RF} 3. implement the soil realisations in the FE model and run the FEA → t_{FEA} 4. compute the uniaxial capacities and eventually plot the histogram with a log-normal distribution to analyse the data	3. compute the operative undrained shear strengths, $s_u^{(a)}$ 4. compute the best-fit shape parameter, $f_s^{(a)}$, of the log-normal distribution of $s_u^{(a)}$ 5. scale to the distribution of the uniaxial capacities with: N_{cV}=11.8; N_{cH}=3.22; N_{cM}=1.65	2. compute the shape parameter, $f_s^{(a)}$, with the sparse PCE 3. scale to the distribution of the uniaxial capacities with: N_{cV}=11.8; N_{cH}=3.22; N_{cM}=1.65
total computational time = $t_{RF} + t_{FEA}$	total computational time = t_{RF}	total computational time ≈ 0
tasks: - random field modelling - finite element modelling	tasks: - random field modelling	tasks: - PCE equation

Fig. 10. Summary of the different methods to predict the probabilistic uniaxial capacities of the plate anchor in spatially variable soils.

For Method 1, 300 random realisations of the soil were generated and the respective capacities were determined. A histogram of the results is plotted in Fig. 11a, together with the best-fit log-normal PDF represented by a black continuous curve. Fig. 11b reports the same outcome but in terms of CDF. Using Eq. (13) to fit the data led to a shape parameter of 0.247 and a scale parameter of 87.23kN, which is slightly larger than the deterministic vertical uniaxial capacity. In fact, the results show that for about 40 % of the considered realisations, the deterministic capacity would lead to a somewhat unsafe design – as observed by Cai et al. (2022) for a similar scenario.

The red curves in Fig. 11 reports on the results for Method 2. Here, the operative $s_u^{(a)}$ was computed and the distribution fitted using Eq. (13), resulting in a shape parameter of 0.254 (i.e. + 2.8 % higher than Method 1). The distribution of $s_u^{(a)}$ was then scaled to determine the probability of V_u using the vertical capacity factor defined in Eq. (14). As shown, the estimated PDF and CDF are close to the curves obtained with Method 1.

Finally, the developed sparse PCE was used to predict the shape parameter with the metamodel approach, per Method 3. The PDF and CDF distributions of V_u were computed and plotted as blue curves in Fig. 11a and 11b, respectively. The curves are close approximations of those obtained with Method 1, with negligible error associated with a prediction of the shape parameter of 0.257 (i.e. + 4.05 % higher than Method 1).

While not presented, similar conclusions can be made for horizontal and moment loading of the plate. Overall, this example highlights the potential of the proposed approach, which can yield accurate results with reduced computational cost and complexity.

6. Concluding remarks

This study has investigated the effect of the spatial variability in undrained shear strength on the uniaxial capacity of a deeply embedded plate anchor. It is shown that random realisations of non-stationary fields can be associated with an operative value of undrained shear strength, $s_u^{(a)}$, which is the mean of the operative strengths computed for the three uniaxial conditions of loading ($s_u^{(V)}$, $s_u^{(H)}$, $s_u^{(M)}$). These are defined as the average s_u computed along the (adopted) kinematic

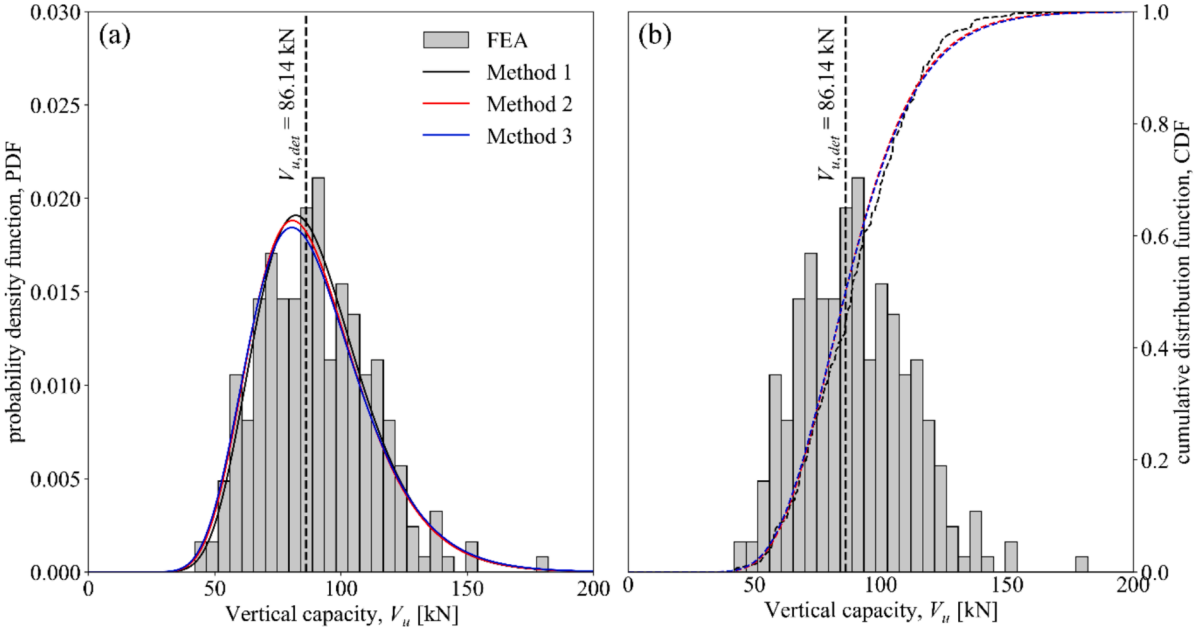

Fig. 11. Probability of failure of the plate anchor under vertical load in $N_R = 300$ spatially variable fields generated by $k(s_u) = 1.2$ kPa/m, $\mathrm{COV}(s_u) = 0.3$, $\theta_z(s_u) = 2.5$ m, computed with the three methods.

failure mechanisms for anchors in homogeneous clay. The study demonstrated that using the operative strength, $s_u^{(a)}$, supports single values of capacity factors. By adopting this finding, it is possible to simply relate the statistical distribution of operative undrained shear strength to the probability of failure of the plate under uniaxial loading.

Key conclusions are as follows:

- The operative soil strengths can be represented using log-normal distributions for a given combination of the input variables that represent the heterogeneity of s_u. The inputs were selected as they can be estimated by offshore site investigation, thus allowing the approach to be extended to practical application.
- The RFE study showed that ultimate uniaxial capacity is significantly influenced by the heterogeneity of s_u, with a widely distributed probability of failure. However, the distribution narrows significantly if the ultimate capacity is divided by the operative strength, leading to approximately constant capacity factors.
- The PCE metamodelling technique allowed accurate approximation of the operative s_u for any combination of the input variables, without having to generate random field.

This work has led to development of an analytical procedure which relates site-specific soil input variables to the probability of failure of the foundation. The procedure has the practical advantage that simple equations are used (i.e. ultimate capacity and PCE equations) without having to run computationally expensive RFE analyses.

While the procedure presented in this paper is likely to have general applicability, it is limited to consideration of a specific foundation geometry and size. Further studies, which encompass plate anchors with a realistic range of dimension, would be required to generalise the approach. Additionally, it would be beneficial to independently consider the effect of the horizontal scale of fluctuation on the anchor response (the current study links vertical and horizontal variability). This would allow for a procedure to be developed that better deals with realistic site heterogeneity in the undrained shear strength.

CRediT authorship contribution statement

Alessio Mentani: Writing – original draft, Methodology, Investigation, Funding acquisition, Formal analysis, Data curation, Conceptualization. **Laura Govoni:** Writing – original draft, Supervision, Project administration, Methodology, Conceptualization. **Christophe Gaudin:** Writing – review & editing, Supervision, Conceptualization. **Phil Watson:** Writing – review & editing, Supervision, Conceptualization. **Yinghui Tian:** Writing – review & editing, Methodology.

Declaration of competing interest

The authors declare that they have no known competing financial interests or personal relationships that could have appeared to influence the work reported in this paper.

Acknowledgement

This work forms part of the activities of the project SEAFLOWER, which has received funding from the European Union's Horizon 2020 research and innovation programme, under the Marie Skłodowska-Curie grant agreement No 891826.

Appendix A

The PCE metamodels presented in this study were developed using Legendre orthonormal polynomials. Given that $P_0(x) = 1$ is the Legendre polynomial in a variable x of degree equal to 0, any sequence of orthornormal polynomials in x can then be determined as:

$$P_{i+1}(x) = (a_i x)P_i(x) + b_i P_{i-1}(x) \tag{A.1}$$

where the two coefficients, a and b, are computed as:

$$a_i = \frac{\sqrt{(2i+1)(2i+3)}}{i+1} \tag{A.2}$$

$$b_i = -\frac{i\sqrt{2i+3}}{(i+1)\sqrt{2i-1}} \tag{A.3}$$

The sparse PCE was built for $n = 3$ input variables ($x_n = \{k(s_u), \mathrm{COV}(s_u), \theta_z(s_u)\}^{\mathrm{T}}$).

As detailed in Fig. 8 and also summarised in Table A.1, the α-coefficients were computed for polynomials up to a maximum degree $p = 6$. The entire equation consists of ten terms as the LAR approach is applied with a cut-off set to $\varepsilon_{cut\text{-}off} = 1{*}10^{-3}$, which reduced the number of significant polynomials.

Table A1
Polynomial basis of the sparse PCE up to maximum degree $p = 6$, and relevant coefficients.

Polynomial	Degree	Coefficient
P_0	0	0.2139
$P_1(x_2)$	1	0.1121
$P_1(x_3)$	1	0.0159
$P_1(x_2)P_1(x_3)$	2	0.0084
$P_2(x_3)$	2	−0.0089
$P_2(x_1)P_1(x_3)$	3	−0.0019
$P_1(x_2)P_2(x_3)$	3	−0.0072
$P_3(x_3)$	3	0.0112
$P_4(x_1)P_1(x_3)$	5	0.0061
$P_2(x_1)P_2(x_2)P_2(x_3)$	6	−0.0022

Data availability

Data will be made available on request.

References

Blatman, G., Sudret, B., 2010. Adaptive sparse polynomial chaos expansion based on least angle regression. J. Comput. Phys. 230, 2345–2367.

Bransby, M.F., Randolph, M.F., 1998. Combined loading of skirted foundations. Géotechnique 48 (5), 637–655.

Cai, Y., Bransby, M.F., Gaudin, C., Tian, Y., 2022. Accounting for soil spatial variability in plate anchor design. ASCE J. Geotech. Geoenviron. Engng. 148 (2), 04021178.

Cami, B., Javankhoshdel, S., Phoon, K.K., Ching, J., 2020. Scale of fluctuation for spatially varying soils: estimation methods and values. ASCE–ASME J. Risk Uncertain. Engng. Syst. A: Civ. Engng. 6 (4), 03120002.

Cassidy, M.J., Uzielli, M., Tian, Y., 2013. Probabilistic combined loading failure envelopes of a strip footing on spatially variable soil. Comp. Geotech. 49, 191–205.

Chen, H., Shen, Z., Wang, L., Qi, C., Tian, Y., 2023. Probabilistic analysis of skirted foundations under combined loading in soils modelled by non-stationary random fields. Ocean Eng. 272, 113791.

Ching, J., Schweckendiek, T., 2021. State-of-the-art review of inherent variability and uncertainty in geotechnical properties and models. ISSMGE Technical Committee 304. International Society of Soil Mechanics and Geotechnical Engineering, London.

Systèmes, D., 2020. Abaqus analysis User's Manual. Providence, RI, USA.

Fenton, G.A., Griffiths, D.V., 2008. Risk assessment in geotechnical engineering. Wiley, Hoboken, NJ.

Elkhatib, S., Randolph, M.F., 2005. The effect of interface friction on the performance of drag-in plate anchors. In: Proc. 5th Int. Symp. on Frontiers in Offshore Geotechnics, Perth, pp. 171–177.

Gaudin, C., O'Loughlin, C.D., Randolph, M.F., Lowmass, A.C., 2006. Influence of the installation process on the performance of suction embedded plate anchors. Géotechnique 56 (6), 381–391.

Gaudin, C., Cassidy, M.J., O'Loughlin, C.D., Tian, Y., Wang, D. and Chow, S., 2017. Recent advances in anchor design for floating structures. In J. S. Chung (Ed.), International Journal of Offshore and Polar Engineering: Proceedings of the 12th ISOPE Pacific-Asia Offshore Mechanics Symposium (1 ed., Vol. 27, pp. 44-53).

Griffiths, D.V., Fenton, G.A., 2001. Bearing capacity of spatially random soil: the undrained clay Prandtl problem revisited. Géotechnique. 51 (4), 351–359.

Hallowell, S.T., Arwade, S.R., Fontana, C.M., DeGroot, D.J., Aubeny, C.P., Diaz, B.D., Myers, A.T., Landon, M.E., 2018. System reliability of floating offshore wind farms with multiline anchors. Ocean Eng. 160, 94–104.

Kumar, Y., Ringenberg, J., Depuru, S.S., Devabhaktuni, V.K., Lee, J.W., Nikolaidis, E., Andersen, B., Afjeh, A., 2016. Wind Energy: trends and enabling technologies. Renew. Sustain. Energy Rev. 53, 209–224.

Le Gratiet, L., Marelli, S., Sudret, B., 2015. Metamodel-Based Sensitivity Analysis: Polynomial Chaos Expansions and Gaussian Processes. In: Ghanem, R., Higdon, D., Owhadi, H. (Eds.), Handbook of Uncertainty Quantification. Springer, Cham.

Li, J., Tian, Y., Cassidy, M.J., 2015. Failure mechanism and bearing capacity of footings buried at various depths in spatially random soil. ASCE J. Geotech. Geoenviron. Engng. 141 (2), 04014099.

Lumb, P., 1966. The variability of natural soils. Can. Geotech. J. 3 (2), 74–97.

Mentani, A., Govoni, L., Bourrier, F., Zabatta, R., 2023. Metamodelling of the load-displacement response of offshore piles in sand. Comput. Geotech. 159 (6), 105490.

Merifield, R.S., Sloan, S.W., Yu, H.S., 2001. Stability of plate anchors in undrained clay. Géotechnique. 51 (2), 141–153.

Murff, J.D. (1994). Limit analysis of multi-footing foundation systems. In Proceedings of the 8th International Conference on Computer Methods and Advances in Geomechanics. Morgantown, May. Edited by H.J. Siriwardane and M.M. Zaman. A. A. Balkema, Rotterdam. Vol. 1, pp. 223–244.

O'Loughlin, C., Neubecker, S. and Gaudin, C. (2018). Anchoring Systems: Anchor Types, Installation, and Design. In Encyclopedia of Maritime and Offshore Engineering (eds J. Carlton, P. Jukes and Y.S. Choo).

O'Neill, M., Bransby, M.F., Randolph, M.F., 2003. Drag anchor fluke-soil interaction in clays. Can. Geotech. J. 40 (1), 78–94.

Phoon, K.K., Kulhawy, F.H., 1999. Characterization of geotechnical variability. Can. Geotech. J. 36 (4), 612–624.

Randolph, M., Gourvenec, S., 2017. Offshore geotechnical engineering. CRC Press, Boca Raton, FL.

Räss, L., Kolyukhin, D., Minakov, A., 2019. Efficient parallel random field generator for large 3-D geophysical problems. Comput. Geosci. 131, 158–169.

Shen, Z., Jin, D., Pan, Q., Yang, H., Chian, S.C., 2020. Probabilistic analysis of strip footings on spatially variable soils with linearly increasing shear strength. Comput. Geotech. 126, 103653.

Shen, Z., Pan, Q., Chian, S.C., Gourvenec, S., Tian, Y., 2023. Probabilistic failure envelopes of strip foundations on soils with non-stationary characteristics of undrained shear strength. Géotechnique 73 (8), 716–735.

Soize, C., Ghanem, R., 2004. Physical systems with random uncertainties: chaos representations with arbitrary probability measure. SIAM J. Sci. Comput. 26 (2), 395–410.

Stanier, S.A., White, D.J., 2019. Enhancement of bearing capacity from consolidation: due to changing strength or failure mechanism? Géotechnique. 69 (2), 166–173.

Sudret, B., 2008. Global sensitivity analysis using polynomial chaos expansions. Reliab. Engng. Syst. Saf. 93 (7), 964–979.

Suryasentana, S.K., Sheil, B.B., Stuyts, B., 2024a. Multifidelity Data Fusion for the Estimation of Static Stiffness of Suction Caisson Foundations in Layered Soil. ASCE J. Geotech. Geoenviron. Engng. 150 (8), 04024066.

Suryasentana, S.K., Sheil, B.B., Stuyts, B., 2024b. Practical approach for data-efficient metamodeling and real-time modeling of monopiles using physics-informed multifidelity data fusion. ASCE J. Geotech. Geoenviron. Engng. 150 (8), 06024005.

Ukritchon, B., Whittle, A.J., Sloan, S.W., 1998. Undrained limit analysis for combined loading of strip footings on clay. ASCE J. Geotech. Geoenviron. Engng. 124 (3), 265–276.

Vulpe, C., Gourvenec, S., Power, M., 2014. A generalised failure envelope for undrained capacity of circular shallow foundations under general loading. Géotechnique Letters. 4, 187–196.

Wu, Y., Zhou, X., Gao, Y., Shu, S., 2020. Bearing capacity of embedded shallow foundations in spatially random soils with linearly increasing mean undrained shear strength. Comput. Geotech. 122, 103508.

Yu, L., Liu, J., Kong, X.J., Hu, Y., 2010. Numerical study on plate anchor stability in clay. Géotechnique. 61 (3), 235–246.

Yi, J.T., Huang, L.Y., Li, D.Q., Liu, Y., 2020. A large-deformation random finite-element study: Failure mechanism and bearing capacity of spudcan in a spatially varying clayey seabed. Géotechnique. 70 (5), 392–405.

Zhang, P., Jin, Y.F., Yin, Z.Y., Yang, Y., 2020. Random forest based artificial intelligent model for predicting failure envelopes of caisson foundations in sand. Appl. Ocean Res. 101, 102223.